Self-assembly of the general membrane-remodeling protein PVAP into sevenfold virus-associated pyramids

Bertram Daum[a,1], Tessa E. F. Quax[b,1], Martin Sachse[c], Deryck J. Mills[a], Julia Reimann[d], Özkan Yildiz[a], Sabine Häder[a], Cosmin Saveanu[e], Patrick Forterre[b], Sonja-Verena Albers[d], Werner Kühlbrandt[a,2], and David Prangishvili[b,2]

[a]Department of Structural Biology, Max Planck Institute of Biophysics, 60438 Frankfurt am Main, Germany; [b]Biologie Moléculaire du Gène chez les Extrêmophiles, [c]Plate-Forme de Microscopie Ultrastructurale, and [e]Génétique des Interactions Macromoléculaires, Institut Pasteur, 75015 Paris, France; and [d]Molecular Biology of Archaea, Max-Planck Institute for Terrestrial Microbiology, 35043 Marburg, Germany

Edited by Wah Chiu, Baylor College of Medicine, Houston, TX, and approved January 27, 2014 (received for review October 11, 2013)

Viruses have developed a wide range of strategies to escape from the host cells in which they replicate. For egress some archaeal viruses use a pyramidal structure with sevenfold rotational symmetry. Virus-associated pyramids (VAPs) assemble in the host cell membrane from the virus-encoded protein PVAP and open at the end of the infection cycle. We characterize this unusual supramolecular assembly using a combination of genetic, biochemical, and electron microscopic techniques. By whole-cell electron cryotomography, we monitored morphological changes in virus-infected host cells. Subtomogram averaging reveals the VAP structure. By heterologous expression of PVAP in cells from all three domains of life, we demonstrate that the protein integrates indiscriminately into virtually any biological membrane, where it forms sevenfold pyramids. We identify the protein domains essential for VAP formation in PVAP truncation mutants by their ability to remodel the cell membrane. Self-assembly of PVAP into pyramids requires at least two different, in-plane and out-of-plane, protein interactions. Our findings allow us to propose a model describing how PVAP arranges to form sevenfold pyramids and suggest how this small, robust protein may be used as a general membrane-remodeling system.

archaea | archeovirus | viral egress

Release of virus particles from infected cells is the last essential step of the viral replication cycle. In the course of this process, virions face the challenging task of crossing the cell envelope. Viruses have developed an arsenal of diverse strategies to overcome this problem. Most bacterial viruses are lytic and induce lysis of the infected cell with help of the holin-endolysin system (1), whereas others disrupt the host cell envelope via inhibition of the murein biosynthesis pathway (2). The morphological and genomic properties of archaeal viruses (3) suggested that their egress from host cells may have unusual traits that are different from those of bacterial viruses. Indeed, although most archaeal viruses exit cells without lysis, some, in particular the *Sulfolobus islandicus* rod-shaped virus 2 (SIRV2) and *Sulfolobus* turreted icosahedral virus (STIV), are lytic and exploit a special mechanism of virion egress (4–8). During the infection cycle of these viruses, pyramidal protrusions with sevenfold rotational symmetry form in the host cell membrane. As the final step of the infection cycle the virus-associated pyramids (VAPs) open outwards along the seams of their seven facets, creating ~100-nm apertures through which the newly formed virions escape from the host cell (4, 7). VAPs consist of multiple copies of an ~10-kDa virus-encoded protein, which we term "PVAP" (Protein forming Virus-Associated Pyramids/SIRV2_P98) (7–9). Surprisingly, PVAP assembles into membrane pyramids even when expressed heterologously in archaeal and bacterial expression systems, demonstrating that no other viral proteins are required for VAP formation (7). The mechanism by which VAPs self-assembles in the membrane remains unknown.

In the present study we used electron cryotomography to investigate morphological features of SIRV2 replication and the formation of VAPs at different time points after infection. By subtomogram averaging, we determined a 3D map of the VAP. This map, in combination with secondary structure predictions of PVAP and the expression of wild-type (WT) *PVAP* or a variety of truncation mutants in archaeal, bacterial and eukaryotic cells allows us to propose a model showing how PVAP arranges to form the sevenfold pyramids. These insights are fundamental for understanding how this mechanism can be exploited as a universal tool to engineer the formation and controlled opening of large pores in biological or artificial lipid bilayers.

Results

SIRV2 Induces Morphological Changes in the Host Cell. We analyzed morphological changes in *S. islandicus* during SIRV2 infection and the time points of VAP formation and opening by whole-cell electron cryotomography at 0.5, 3, 6, and 12 h post infection (h.p.i.). This strategy allowed us to monitor morphological changes at high resolution and to compare these results with previous results obtained by thin-sectioning of chemically fixed cells during the final stages of SIRV2 infection (4). Up to 3 h.p.i. infected cells were indistinguishable from uninfected control cells, and no virions were visible in the cytoplasm (Fig. 1*A*). This finding is in accordance with a previous study, in which we have observed infection of *S. islandicus* by SIRV2 directly in the electron microscope and suggests that SIRV2 does not enter the cell as an intact virus particle (10). Electron-dense

Significance

The *Sulfolobus islandicus* rod-shaped virus 2 (SIRV2) has developed unique mechanisms to penetrate the plasma membrane and S-layer of its host *Sulfolobus islandicus* in order to leave the cell after replication. SIRV2 encodes the 10-kDa protein PVAP, which assembles into sevenfold symmetric virus-associated pyramids (VAPs) in the host cell plasma membrane. Toward the end of the viral replication cycle, these VAPs open to form pores through the plasma membrane and S-layer, allowing viral egress. Here we show that PVAP inserts spontaneously and forms VAPs in any kind of biological membrane. By electron cryotomography we have obtained a 3D map of the VAP and present a model describing the assembly of PVAP into VAPs. Our findings open new avenues for a large variety of biotechnological applications.

Author contributions: S.-V.A., W.K., and D.P. designed research; B.D., T.E.F.Q., M.S., D.J.M., J.R., Ö.Y., S.H., and C.S. performed research; W.K. and D.P. contributed new reagents/analytic tools; B.D., T.E.F.Q., Ö.Y., P.F., S.-V.A., W.K., and D.P. analyzed data; and B.D., T.E.F.Q., W.K., and D.P. wrote the paper.

The authors declare no conflict of interest.

This article is a PNAS Direct Submission.

Data deposition: The map reported in this paper has been deposited in the Electron Microscopy Data Bank, www.emdatabank.org (accession no. 5844).

[1]B.D. and T.E.F.Q. contributed equally to this work.

[2]To whom correspondence may be addressed. E-mail: werner.kuehlbrandt@biophys.mpg.de or david.prangishvili@pasteur.fr.

This article contains supporting information online at www.pnas.org/lookup/suppl/doi:10.1073/pnas.1319245111/-/DCSupplemental.

globules (~100 nm), similar to those reported for *Sulfolobus solfataricus* cells (11), were the only conspicuous features in the cytoplasm of controls and infected cells (Fig. 1*A*),. However, each cell, infected or not, contained one or a few of these globules, which therefore are unrelated to virus replication. Their size and density above the cytoplasmic background indicates that they may be storage granules (12).

At 3–6 h.p.i., about half way through the infection cycle, newly assembled virions became visible in the cytoplasm. as described earlier (4). They were organized in up to three bundles per cell, each consisting of roughly 50 rod-shaped particles (Fig. 1*B*). Starting at 3 h.p.i., VAPs of various size formed in the plasma membrane of the host cells, and most of these VAPS had penetrated the S-layer (Figs. 1*B* and 2 *A*–*D*). Each cell contained on average about 10 VAPs. The height of the VAPs (measured from the membrane to the tip of the pyramid) ranged from ~20–150 nm. At an early stage of formation the VAPs in the plasma membrane had not yet punctured the S-layer of the host cell (Fig. S1), but they already had the distinct features of hollow heptagonal pyramids, corroborating the earlier assumption that VAPs grow from the base by gradual expansion of their triangular facets (7). Very occasionally, VAPs contained a spherical storage granule (Fig. 2*C*). These granules likely correspond to the previously described intrapyramidal bodies (IPB) in STIV-induced VAPs (11). Analysis of cells at distinct time points post infection showed that at 6 h.p.i. a number of VAPs had opened. The fraction of open VAPs increased until at 12 h.p.i. all VAPs had unfolded like the petals of a flower (Figs. 1*C* and 2 *E*–*H*). The VAPs appeared to open as the pyramidal structures broke along the seams of the triangular pyramid faces (Fig. 2*F*). The VAP facets curved outwards with counterclockwise handedness when viewed from the cell exterior (Fig. 2*F*), as suggested by electron micrographs of isolated VAPs (7). As the VAPs opened, the virion bundles disintegrated, and individual virions diffused into the medium through the open VAPs (Fig. 3).

VAP Structure. The shape of isolated VAPs has been investigated previously by negative staining and electron microscopy (7). To gain insight in the structure of VAPs in situ, closed or open VAPs were imaged by whole-cell electron cryotomography (Fig. 4 *A*–*C*). The triangular faces of all VAPs appeared to consist of two distinct layers, irrespective of their conformation or stage of assembly. The outer layer (~4.5 ± 1 nm) was continuous with and indistinguishable from the cell membrane. The inner layer had a thickness of ~4.0 ± 1 nm (Fig. 4). The center-to-center distance between the two layers was 10.0 ± 1 nm, leaving a 5.8 ± 1 nm gap of lower density. At the base of each VAP, the inner layer extended up to 15 nm beyond the outer layer into the cytoplasm. These observations suggest that the inner layer consists of a protein sheet that is attached and runs parallel to the cytoplasmic membrane surface (Fig. 4).

To verify that both layers of the VAP consist only of PVAP protomers, we analyzed archaeal (*Sulfolobus acidocaldarius*) or bacterial (*Escherichia coli*) *PVAP* expression mutants constructed in a previous study (7). Whole-cell electron cryotomography of transformed cells revealed the distinctive two layers in all VAPs (Fig. 4*C* and Fig. S2), indicating that both layers consist solely of PVAP (Fig. S3).

Subtomogram Averaging of VAPs. A 3D map of the VAP was obtained by averaging 57 tomographic subvolumes of closed VAPs in the membrane of *PVAP*-expressing *E. coli* cells. Sections through the averaged volume parallel to the membrane showed clear sevenfold symmetry (Fig. S3), which was applied to the final average to improve the signal-to-noise ratio further (Fig. 4 *D*–*K* and Movie S1). The local resolution estimated by the program ResMap (13) was between 36 and 58 Å, with a mean resolution of ~43Å (Fig. S4). Because VAPs come in different sizes, only the upper parts of the pyramids, to a height of ~62 nm and an outer diameter of ~96 nm, were used for averaging. At the tip, the inner opening angle of the pyramid was ~80° (Fig. 4*D*). As observed in the raw tomograms, the structure consisted of two layers (Fig. 4 *D*, *E*, and *I*–*K*). The outer layer formed a continuous envelope, consisting of seven triangular facets (Fig. 4 *F*–*K*). As seen from the outside, the facets had a perceptible counterclockwise handedness (Fig. 4*F*), and each facet was slightly convex toward the inside (Fig. 4 *F, G, J,* and *K*). The angle at the tip of the triangular facets was 35°, in accordance with previous measurements on isolated VAP fragments (7). Overall, the entire structure had the appearance of a tent or teepee (Fig. 4 *G*). The inner, cytosolic layer of the pyramid consisted of seven triangular sheets parallel to the membrane on the outside (Fig. 4 *I*–*K*). Cross-sections through the sevenfold averaged volume revealed narrow connecting densities between the two layers of the pyramid, suggesting that they are physically linked (Fig. 4*K*).

Membrane Remodeling by PVAP. In silico secondary structure predictions (14) and hydrophobicity analysis (15) of PVAP suggest that the protein consists of an N-terminal transmembrane helix (residues 5–34), followed by three hydrophilic α-helices of two to three turns each separated by short linker regions (Fig. S5). The PSORT-server (16) indicated that PVAP does not contain a presequence. This result is consistent with a previous study of the N-terminal amino acid sequence of purified PVAP of SIRV2 with Edman degradation, which did not indicate a cleavable signal sequence (9). Thus, we assumed that the hydrophobicity of its predicted N-terminal transmembrane segment drives the spontaneous insertion of PVAP into the lipid bilayer. To test this hypothesis, *PVAP* was expressed in the *Saccharomyces cerevisiae*, a eukaryotic organism. Cells were harvested 16 h after induction of *PVAP* expression and were high-pressure frozen and freeze-substituted. In addition, sections prepared by the Tokuyasu method (17) were immunolabeled with antibodies raised against PVAP. All samples were analyzed by transmission electron microscopy. Surprisingly, VAPs were found

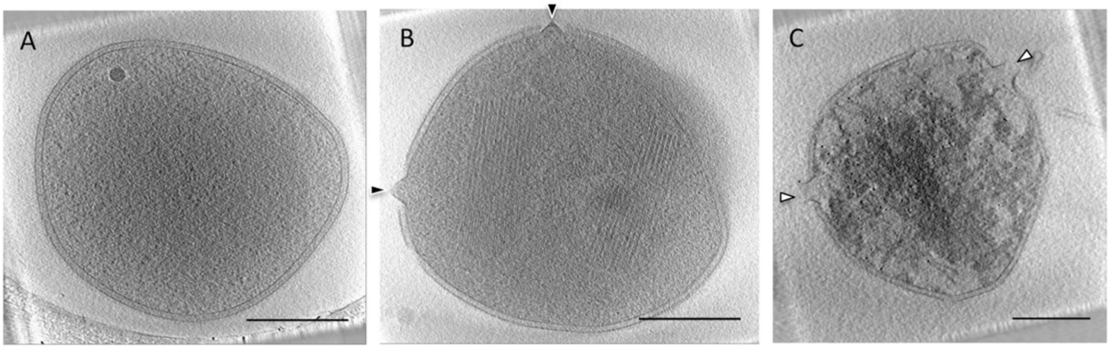

Fig. 1. Morphological changes of *S. islandicus* during infection with SIRV2. Tomographic slices of typical archaeal cells at 0.5 (*A*), 3–6 (*B*), and 9 (*C*) h.p.i. with SIRV2. Black arrowheads indicate closed VAPs; white arrowheads indicate open VAPs. (Scale bars, 500 nm.)

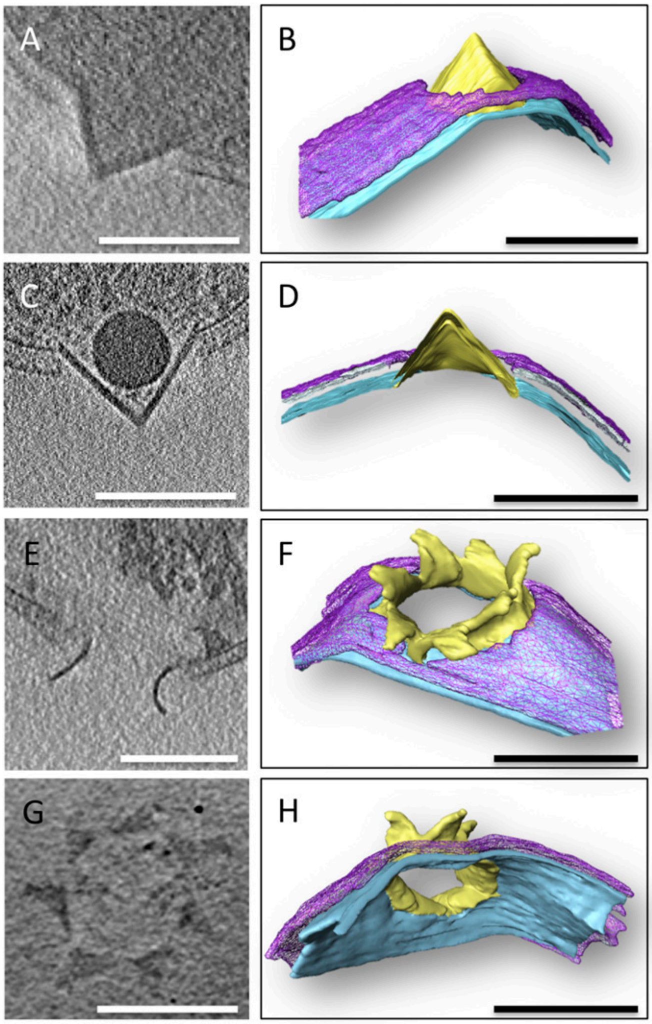

Fig. 2. VAPs in closed and open conformation. Tomographic slice (*A*, *C*, *E*, and *G*) and segmented, surface-rendered volumes (*B*, *D*, *F*, and *H*) of VAPs in the membrane of SIRV2-infected *S. islandicus* cells. VAPs are either closed (*A*–*D*) or open (*E*–*H*). The S-layer is purple, the cell membrane is blue, and the VAP is yellow. (Scale bars, 200 nm.)

in most, if not all, cellular membranes. In size and appearance, the pyramids were indistinguishable from those that assembled in *E. coli* after PVAP expression or in *S. islandicus* after SIRV2 infection. PVAP-specific antibodies labeled VAPs in the nuclear envelope, the endoplasmic reticulum, Golgi apparatus, intracellular vesicles, and mitochondria (Fig. 5).

Role of PVAP Domains in VAP Assembly. To identify which parts of the PVAP are required for VAP assembly, truncated mutants lacking the last 10, 20, 30, 40, or 70 C-terminal residues (*ΔC10, ΔC20, ΔC30, ΔC40*, or *ΔC70*, respectively) were constructed (Fig. 6). Electron microscopy analysis of *E. coli* cells transfected with these constructs revealed VAPs only in case of the *ΔC10* mutant (Fig. 6*)*.

In contrast, VAPs did not form after truncation of 20–70 C-terminal residues (PVAP*ΔC20*, *ΔC30*, *ΔC40*, or *ΔC70*, Fig. 6) corresponding to one to three C-terminal α-helical segments. Instead, expression of these constructs resulted mostly in protein aggregates. In addition, constructs lacking 20–40 C-terminal residues caused the inner membrane of *E. coli* to form large invaginations, suggesting that these variants still interact with the membrane (Fig. 6*B*). The effect was most pronounced for PVAPΔC20. In contrast, PVAPΔC70 did not produce any membrane invaginations (Fig. 6*B*).

Expression of a *PVAP* construct lacking the predicted N-terminal transmembrane helix (*PVAPΔN30*) likewise did not result in VAP formation. There was no sign of any interaction with the membrane (Fig. 6*B*), indicating that the N-terminal transmembrane domain is indeed required for membrane insertion of PVAP protomers.

We asked if the PVAP transmembrane domain is essential for VAP formation or could be replaced by any other transmembrane domain. To characterize the role of the PVAP transmembrane domain in VAP formation, we constructed a chimera by fusing the *E. coli* flagellar regulator *Flk*, a gene encoding a single transmembrane helix inner membrane protein (18), to *PVAPΔN30*, replacing the N-terminal transmembrane helix (residues 1–30) of PVAP (18). After expression, this fusion construct (PVAPtmFlk) was indeed inserted into the membrane, as judged by Western blot analysis of cell fractions with SIRV2-PVAP antibody (Fig. S6). However, there was no evidence of VAPs in these cells (Fig. 6*B*).

Taken together these findings indicate that the N-terminal domain is essential for membrane insertion of PVAP and for the interaction between PVAP protomers, which results in the assembly of a protein sheet on the inner membrane surface. The C-terminal domain of PVAP (except the last 10 residues, which are predicted to be disordered) is required for VAP formation. Without this domain, the protein aggregates instead of forming VAPs.

PVAP Oligomers. To characterize the oligomerization of PVAP in vitro, we fused a His-tag to the C terminus and expressed the protein heterologously in *E. coli*. Isolated membranes were solubilized with the detergent *N*-laurylsarcosine. PVAP was purified by nickel affinity chromatography and size-exclusion chromatography. The single peak in the gel filtration profile corresponds to a molecular mass of ~70 kDa (Fig. S7). SDS/PAGE analysis of peak fractions shows discrete PVAP bands at ~10, 20, 30, and 70 kDa (Fig. S7), indicating that in detergent solution PVAP forms different oligomers, the largest of which is most likely a heptamer. A PVAP heptamer also is suggested by gel filtration chromatography.

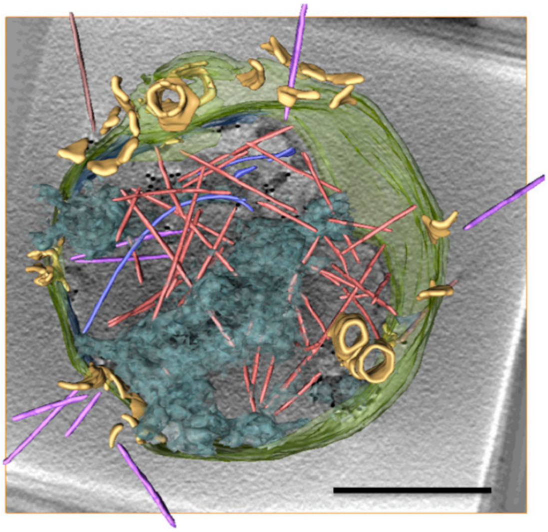

Fig. 3. SIRV2 virion egress. Rendered tomographic volume of a SIRV2-infected *S. islandicus* cell, 12 h.p.i. SIRV2 virions (orange, brown, and purple) are released through open VAPs (yellow) that create ~100-nm apertures in the plasma membrane and S-layer (green). Virions inside the cell are orange; virions escaping from the cell are purple; virions outside the cell are brown. Viral or host DNA is transparent blue. (Scale bar, 500 nm.)

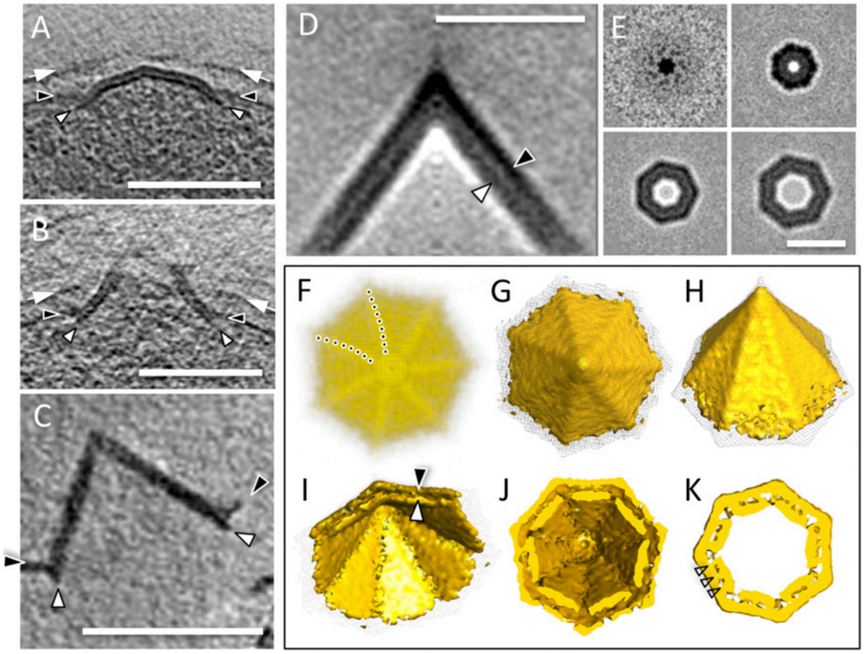

Fig. 4. VAP structure. Tomographic slices through closed (*A*) and open (*B*) SIRV2-induced VAPs of *S. islandicus* and VAPs formed after PVAP expression in *E. coli* (*C*), indicating two layers. One layer is continuous with the cell membrane (black arrowheads), and the other (white arrowheads) forms a sheet at the cytoplasmic surface of the membrane. VAPs in *S. islandicus* protrude through the S-layer (white arrows). (*D*–*K*) A 3D map of VAP obtained by subtomogram averaging, with sevenfold symmetry applied. Tomographic slice perpendicular to the pyramid base (*D*) and successive tomographic slices parallel to the base (*E*) show the two layers in the walls of the pyramid. (*F*) Top view of the 3D map in solid representation shows that the edges of the seven pyramidal facets are slightly curved counterclockwise (dotted lines). (*G*–*K*) Different orientations of the 3D map in surface representation. Transparent mesh and golden surface show different threshold levels. Black and white arrowheads indicate the outer and inner layer, respectively. Open arrowheads indicate connections between inner and outer layers of the VAP. (Scale bars, 200 nm in *A*–*C*, 50 nm in *D* and *E*.)

Discussion

The VAP, an archeoviral egress structure that takes the shape of a large, sevenfold pyramid in the host membrane, is without parallel in biology. It consists of multiple copies of PVAP, a 10-kDa membrane protein, which forms VAPs in the membrane, evidently without the need for any other cellular component.

How does the 10-kDa PVAP assemble to form sevenfold pyramids in the membrane? To address this question, we investigated the VAP structure itself by electron cryotomography and have studied the membrane insertion and biochemical properties of PVAP. We have demonstrated that PVAP forms VAPs in archaeal, bacterial, and eukaryotic membranes, into which it inserts indiscriminately, and that, with the exception of the last 10 C-terminal residues, the entire length of the protein is required for VAP assembly. Finally, we have shown that PVAP forms oligomers, most likely heptamers, in detergent solution.

PVAP is a Universal Membrane Remodeling System. Sequence analysis of PVAP suggested that the protein does not contain a signal sequence and thus most likely integrates spontaneously into the archaeal membrane. A similar mechanism of membrane insertion has been found for tail-anchored (TA) proteins (19) and for bacterial pore-forming toxins (bPTFs) (20). TA proteins are indigenous proteins that contain a single C-terminal transmembrane segment. They are inserted into their target membrane in a Sec-independent but organelle-specific manner, occasionally aided by cytoplasmic chaperones (19). Similar to PVAP, bPTFs are expressed as monomers and insert into the target membrane, where they assemble into pore-forming oligomers, either to kill other bacteria or, in the case of pathogens, to lyse the host membrane and thus aid bacterial proliferation (20).

Overexpression of *PVAP* in the archaeon *S. acidocaldarius*, the bacterium *E. coli*, and the eukaryote *S. cerevisiae* resulted in the formation of VAPs in the plasma membranes of all hosts. Even more remarkably, VAPs were observed in virtually all cellular membranes of the eukaryote *S. cerevisiae*, including the nuclear envelope, the endoplasmic reticulum, the mitochondrial outer membrane, and the plasma membrane. This observation demonstrates that, in contrast to other known types of proteins that integrate into membranes, PVAP is able to insert into practically any biological lipid bilayer solely by virtue of its N-terminal transmembrane segment. Once inserted into the bilayer, it forms sevenfold pyramids, irrespective of fundamental differences in lipid or protein composition of the target membrane. These characteristics render PVAP a unique, universal membrane remodeling tool.

Supramolecular Organization of VAPs. Whole-cell electron cryotomography and subtomogram averaging revealed that the VAPs consist of two layers of roughly equal thickness in all endogenous

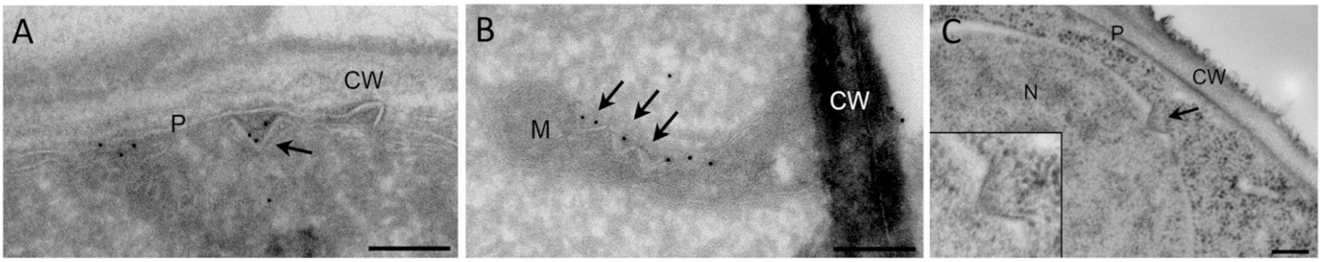

Fig. 5. VAP formation in *S. cerevisiae*. *PVAP* expression in *S. cerevisiae* causes VAP formation in various cellular membranes. (*A* and *B*) Immunolabeling of thawed cryosections with anti-PVAP antibodies. (*A*) VAP in the endoplasmic reticulum. (*B*) VAPs in mitochondrial membranes (*C*) Freeze-substituted cell with VAP in the nuclear envelope. The inset shows an enlarged VAP. CW, cell wall; M, mitochondrion; N, nucleus; P, plasma membrane. Arrows indicate VAPs. (Scale bars, 200 nm.)

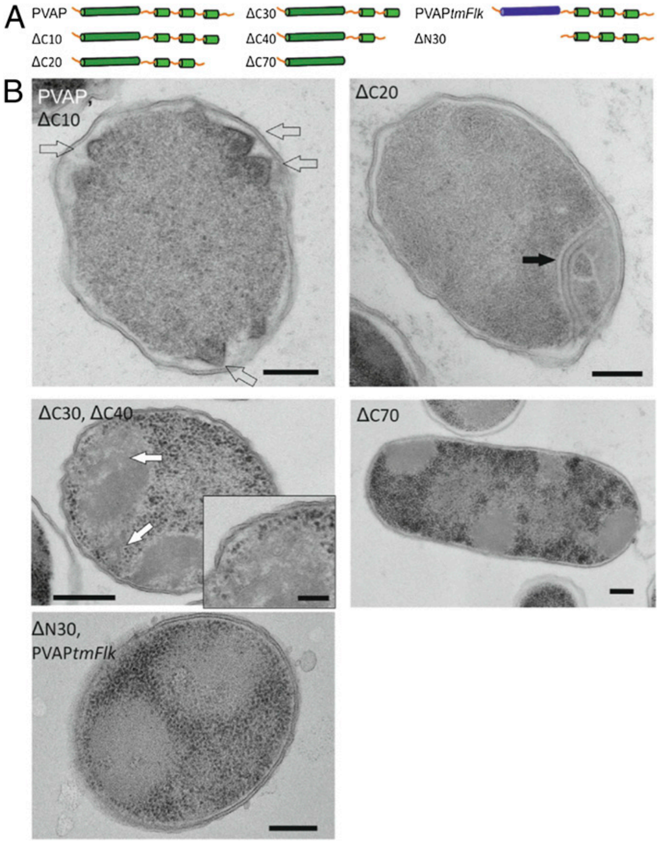

Fig. 6. Expression of truncated variants of *PVAP* in *E. coli*. (*A*) Schematic representation of WT PVAP and its truncated variants. PVAP*ΔC10*, PVAP*ΔC20*, PVAP*ΔC30*, PVAP*ΔC40* 40, and PVAP*ΔC70*, the truncated variants of PVAP lacking the last 10, 20, 30, 40, or 70 C-terminal residues, respectively; PVAP*tmFlk*, the PVAP variant in which the transmembrane segment was replaced by that of the *E. coli* membrane protein Flk; and ΔN30, where the transmembrane segment of PVAP was deleted entirely. (*B*) Electron micrographs of thin sections through *E. coli* cells expressing PVAP constructs as in *A*. VAPs (open arrows) and invagination of the membrane (black arrow) are shown. (Scale bars, 200 nm; scale bar in *Inset*, 100 nm.)

and heterologous expression hosts. The outer layer was continuous with the plasma membrane, whereas the inner layer formed a discontinuous sheet at the cytoplasmic membrane surface. Because PVAP must insert with its N-terminal transmembrane segment into the plasma membrane, the outer layer most likely consists of multiple copies of this part of PVAP plus interspersed membrane lipid. In turn, the cytoplasmic protein sheet must consist of the tightly associated C-terminal domains of the protein. The low-density region between the two layers then would account for the linker region between the cytoplasmic domains and the N-terminal transmembrane segments (Fig. 7*A*).

Recently it was suggested that the opening of STIV-induced VAPs depends on polymerization of Endosomal Sorting Complexes Required for Transport (ESCRT)-III homologs, resulting in the stripping of VAPs from their cytoplasmic membrane (21). Our observation that the outer layer of the double-layered VAP structure is continuous with the plasma membrane (Fig. 4) does not support this model. Moreover, global analysis of host gene expression during the SIRV2 infection cycle documented that ESCRT-III–like proteins were down-regulated in infected cells (22). Thus, it is possible, although not very likely, that mechanisms of VAP opening differ in SIRV2- and STIV-infected cells.

Our tomograms of closed and open VAPs throw some light on the mechanism by which the pyramids open to facilitate viral egress. The seven edges of the closed pyramid are slightly curved in a right-handed fashion (Fig. 4*F*). In the open state, the edges of the seven individual facets are curved in the same way (Fig. 4*F*). In the open VAP, each facet curls outwards (Fig. 4*F*). These observations suggest that in the closed state the VAP structure is under mechanical tension. This tension likely provides the energy required for VAP opening. Because the tip of the VAP displays the point of strongest membrane curvature in the whole assembly, it most likely serves as predetermined breaking point at which the pyramid would begin to unfold along its seams.

VAP Assembly and Opening. We propose a model for VAP assembly (Fig. 7). Upon synthesis in the cytosol, PVAP integrates spontaneously into the cell membrane, depending solely on the hydrophobicity of its N-terminal transmembrane helix segment. In the membrane, tight interactions between PVAP protomers result in the formation of protein sheets that consist of the observed two layers. We propose that this interaction involves both the N-terminal transmembrane helices and the C-terminal hydrophilic PVAP domains, as indicated by the expression of truncation constructs.

To assemble into a pyramid instead of a flat sheet, at least two different kinds of interactions between PVAPs are necessary, one in-plane interaction within the triangular facets and one out-of-plane interaction at the edges of the pyramid. The interaction at the edges is most likely weaker than the in-plane interaction, so that the pyramids open along these lines. Because all VAPs observed in *S. islandicus* or in heterologous systems grow to roughly the same size, the expansion of VAP must be constrained in some way.

At present it is unknown whether the pyramids are built in a one-by-one self-assembly process from individual PVAP protomers or whether, upon membrane insertion, the protomers assemble into heptamers that then combine into pyramids in a second stage of assembly. The prior formation of heptamers in the membrane is suggested by the gel filtration experiments, which show one homogenous peak of ∼70 kDa in detergent solution. Given that detergent mimics the hydrophobic membrane environment, it is likely that the same interactions that give rise to the heptamer in a detergent micelle also would

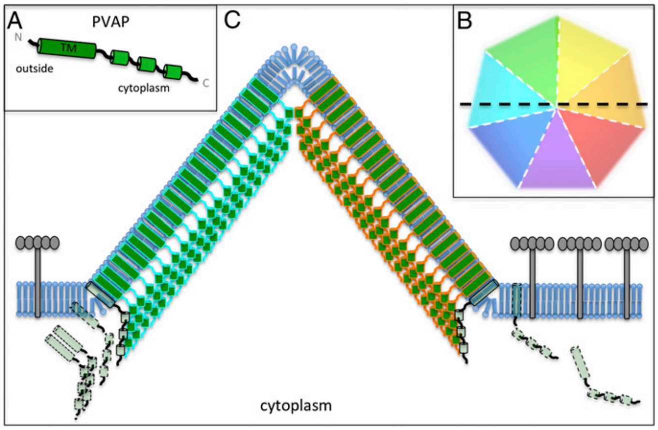

Fig. 7. Model of VAP assembly. (*A*) Predicted secondary structure of PVAP with an N-terminal transmembrane helix and three short C-terminal α-helices. (*B*) Schematic top view of the VAP with its seven facets shown in different colors. Strong interactions between individual PVAP protomers stabilize the integrity of each facet, whereas weak interactions at the seams (white dashed lines) between two neighboring facets form predetermined break points. The black dashed line indicates the cross-section through the VAP in *C*. (C) PVAP protomers (green) insert spontaneously into the plasma membrane (blue), with the short C-terminal helices exposed to the cytoplasm. Close contacts between PVAP molecules in each facet (aqua and orange outline) exclude S-layer proteins (gray) and combine into a protein sheet below the plasma membrane. The addition of PVAP units at the base pushes the pyramid outwards.

promote the formation of heptamers in the membrane, which thus may be the building blocks of the pyramids.

VAP opening presumably involves a host or virus-specific factor, because the pyramids open only in virus-infected *Sulfolobus* cells but remain closed in PVAP-expressing bacteria and yeast. Once the mechanism that triggers VAP opening is elucidated, this system could be used to introduce ∼100-nm apertures in any lipid bilayer. VAPs then might be used for targeted drug delivery, releasing compounds from liposomes upon a specific signal. In addition, the PVAP transmembrane domain has the ability to insert into all types of biological membranes and therefore may be fused to proteins that otherwise cannot be reconstituted into lipid bilayers. This system thus has interesting potential applications in basic research, biotechnology, and therapy.

Materials and Methods

Virus and Host Strains. *S. islandicus* LAL 14/1 cells were grown, synchronized, and infected with SIRV2 as described previously (7) and in *SI Materials and Methods*.

Plasmid Constructs and Transformation of *S. acidocaldarius*. SIRV2_ORF98 (National Center for Biotechnology Information RefSeq ID: NP_666583) was amplified from SIRV2 genomic DNA and cloned into the pSVA1450 plasmid behind an araS promoter, which yielded pTQ26. pTQ26 was transformed to *S. acidocaldarius* M31 as described in *SI Materials and Methods*.

Plasmid Constructs and Transformation of *E. coli*. SIRV2_ORF98 was amplified from SIRV2 genomic DNA with different primers resulting in 3′-truncated PCR products of 267, 237, 207, 177, and 87 bp. A 5′ truncation of ORF98 was created by amplification of a 216-bp product starting at position 81. The same sequence was fused with the 75-bp transmembrane segment of the *E. coli Flk* gene as described in *SI Materials and Methods*. All *PVAP* gene mutants were cloned into the T7 promoter-driven expression vector pSA4. Expression was induced with isopropyl β-D-1-thiogalactopyranoside (IPTG). Analysis of *PVAP*-expressing cultures by high-pressure freezing, freeze-substitution, and Western blotting was performed as described in refs. 7 and 9.

Plasmid Constructs and Transformation of *S. cerevisiae*. *SIRV2_ORF98* was amplified from SIRV2 genomic DNA and cloned in the expression vector pCM190. *S. cerevisiae* was transformed with this plasmid. A preculture was grown in selective medium as described in *SI Materials and Methods*. After 1 d, cells were diluted 1/1,000 in medium without doxycycline.

Immunoelectron Microscopy. Yeast cells were fixed, washed, and pelleted in gelatin, and the gelatin pellet was solidified on ice and cut into small blocks as described in *SI Materials and Methods*. These blocks were infiltrated with 2.3 M sucrose, mounted on aluminum pins, and frozen in liquid nitrogen. Thin sections were cut and picked up in a 1:1 mixture of 2.3 M sucrose and 2% (wt/vol) methylcellulose. Labeling for PVAP was done as described previously (7).

High-Pressure Freezing and Freeze-Substitution. *E. coli* cells were taken up in cellulose capillary tubes, and *S. cerevisiae* cultures were concentrated by filtration. Samples were high-pressure frozen, and freeze-substitution was performed in anhydrous acetone containing 2% (wt/vol) osmium tetroxide. Afterwards the samples were washed with dry acetone and embedded stepwise in EPON (Agar 100 resin; Agar Scientific). After heat polymerization thin sections were cut, collected on 200-mesh Formvar-coated copper grids, and poststained as described in *SI Materials and Methods*. Images were recorded with a JEOL 1010 electron microscope equipped with an Olympus Keen View camera.

Whole-Cell Cryotomography. *S. islandicus* cells were harvested, concentrated by low-speed centrifugation, and plunge-frozen. *E. coli* cells overexpressing *PVAP* were harvested under the same conditions, washed once in 50 mM Tris, 300 mM NaCl, pH7, and plunge-frozen in the same buffer. Before freezing, suspensions were mixed with an equal volume of 10-nm colloidal protein-A gold suspension. Tomograms were recorded with a Polara G2 Tecnai field emission transmission electron microscope equipped with a Gatan Tridiem energy filter and a 2 × 2 k CCD camera. Tomographic tilt series of zero-loss filtered images were recorded, and tomograms reconstructed as described in *SI Materials and Methods*.

Subtomogram Averaging. For subtomogram averaging of VAPs, 57 pyramid volumes were cut out from a single tomogram of an *E. coli* cell overexpressing PVAP and were aligned, and averaged applying sevenfold rotational symmetry using the PEET software as described in *SI Materials and Methods*. The resolution of the map was estimated using the ResMap software (13).

PVAP Purification. A codon-optimized *SIRV_ORF98* gene was synthetized and inserted in the plasmid pET26b. *E. coli* BL21DE3/Rosetta/pLysS cells were transformed with this plasmid. Protein expression was induced with 1 mM IPTG. After 2 h, cells were pelleted, resuspended in lysis buffer, and disrupted with a Microfluidizer. The membrane fraction was pelleted by centrifugation and diluted in 50 mM Tris (pH 7.0), 300 mM NaCl to a protein concentration of 5 mg/mL. Then 1.5% (vol/vol) *N*-laurylsarcosine was added. After high-speed centrifugation the supernatant was loaded onto a Ni-NTA column followed by several washing steps. The protein was eluted in buffer containing 500 mM imidazole and concentrated using Amicon spin columns with a 30-kDa cutoff before loading onto a gel filtration column, as described in more detail in *SI Materials and Methods*.

ACKNOWLEDGMENTS. We thank John van der Oost and Alain Jacquier for helpful discussions and Alp Kuckelbir for help with ResMap. D.P. and T.E.F.Q. received financial support from L'Agence Nationale de la Recherche. W.K. and B.D. received financial support from the Max Planck Society.

1. Krupovic M, Bamford DH (2008) Holin of bacteriophage lambda: Structural insights into a membrane lesion. *Mol Microbiol* 69(4):781–783.
2. Bernhardt TG, Wang IN, Struck DK, Young R (2002) Breaking free: "Protein antibiotics" and phage lysis. *Res Microbiol* 153(8):493–501.
3. Prangishvili D (2013) The wonderful world of archaeal viruses. *Annu Rev Microbiol* 67: 565–585.
4. Bize A, et al. (2009) A unique virus release mechanism in the Archaea. *Proc Natl Acad Sci USA* 106(27):11306–11311.
5. Brumfield SK, et al. (2009) Particle assembly and ultrastructural features associated with replication of the lytic archaeal virus sulfolobus turreted icosahedral virus. *J Virol* 83(12):5964–5970.
6. Prangishvili D, Quax TE (2011) Exceptional virion release mechanism: One more surprise from archaeal viruses. *Curr Opin Microbiol* 14(3):315–320.
7. Quax TE, et al. (2011) Simple and elegant design of a virion egress structure in Archaea. *Proc Natl Acad Sci USA* 108(8):3354–3359.
8. Snyder JC, Brumfield SK, Peng N, She Q, Young MJ (2011) Sulfolobus turreted icosahedral virus c92 protein responsible for the formation of pyramid-like cellular lysis structures. *J Virol* 85(13):6287–6292.
9. Quax TE, Krupovic M, Lucas S, Forterre P, Prangishvili D (2010) The Sulfolobus rod-shaped virus 2 encodes a prominent structural component of the unique virion release system in Archaea. *Virology* 404(1):1–4.
10. Quemin ER, et al. (2013) First insights into the entry process of hyperthermophilic archaeal viruses. *J Virol* 87(24):13379–13385.
11. Fu CY, et al. (2010) In vivo assembly of an archaeal virus studied with whole-cell electron cryotomography. *Structure* 18(12):1579–1586.
12. Iancu CV, et al. (2010) Organization, structure, and assembly of alpha-carboxysomes determined by electron cryotomography of intact cells. *J Mol Biol* 396(1):105–117.
13. Kucukelbir A, Sigworth FJ, Tagare HD (2014) Quantifying the local resolution of cryo-EM density maps. *Nat Methods* 11(1):63–65.
14. Sapay N, Guermeur Y, Deléage G (2006) Prediction of amphipathic in-plane membrane anchors in monotopic proteins using a SVM classifier. *BMC Bioinformatics* 7:255.
15. Krogh A, Larsson B, von Heijne G, Sonnhammer EL (2001) Predicting transmembrane protein topology with a hidden Markov model: Application to complete genomes. *J Mol Biol* 305(3):567–580.
16. Nakai K, Kanehisa M (1991) Expert system for predicting protein localization sites in gram-negative bacteria. *Proteins* 11(2):95–110.
17. Tokuyasu KT (1973) A technique for ultracryotomy of cell suspensions and tissues. *J Cell Biol* 57(2):551–565.
18. Borgese N, Righi M (2010) Remote origins of tail-anchored proteins. *Traffic* 11(7): 877–885.
19. Borgese N, Fasana E (2011) Targeting pathways of C-tail-anchored proteins. *Biochim Biophys Acta* 1808(3):937–946.
20. Bischofberger M, Iacovache I, van der Goot FG (2012) Pathogenic pore-forming proteins: Function and host response. *Cell Host Microbe* 12(3):266–275.
21. Snyder JC, Samson RY, Brumfield SK, Bell SD, Young MJ (2013) Functional interplay between a virus and the ESCRT machinery in archaea. *Proc Natl Acad Sci USA* 110(26): 10783–10787.
22. Quax TE, et al. (2013) Massive activation of archaeal defense genes during viral infection. *J Virol* 87(15):8419–8428.